Brodogradnja Volume 76 Number 2 (2025) 76207

journal homepage: www.brodogradnja.fsb.hr

Brodogradnja

An International Journal of Naval Architecture and
Ocean Engineering for Research and Development

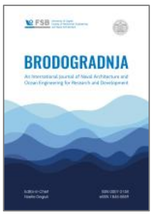

Study on filter clogging and filtration performance evaluation of Ballast Water Management System (BWMS) using analytical and numerical methods

Gang Nam Lee[1], *Tien Trung Duong*[2], *Sangho Park*[3], *Mansoo Kim*[3], *and Kwang Hyo Jung*[2*]

[1]*Department of Ocean System Engineering, Jeju National University, Korea*
[2]*Department of Naval Architecture and Ocean Engineering, Pusan National University, Korea*
[3]*Machinery System part, S&SYS Co., Ltd. Korea*

ARTICLE INFO

Keywords:

Ballast water management system (BWMS)

Filter

Clogging

Total suspended solid (TSS)

Computational fluid dynamics (CFD)

ABSTRACT

Filter clogging is a critical issue in ballast-water management systems (BWMSs) and is caused by the accumulation of sediment deposits and particles in water, particularly under high total suspended solid (TSS) conditions. Despite its significance, studies focusing on the prediction and prevention of clogging, as well as detailed investigations into its mechanisms, remain limited. In this study, an analytical method based on Darcy's law is devised to predict clogging occurrences and filter performance is evaluated via computational fluid dynamics (CFD) simulations. Additionally, a coupled CFD-discrete element method (DEM) approach is employed to investigate clogging mechanisms at the microscopic level, thus providing detailed insights into particle behaviour and fluid dynamics. The results show that clogging occurred rapidly under high-TSS conditions and that the estimated clogging time closely matched the analytical predictions and CFD simulations. Results of CFD-DEM simulation show that larger particles initially obstructed screen pores, followed by a rapid surface coverage, which ultimately increased the pressure drop significantly. The proposed methods offer a reliable framework for evaluating BWMS filter performance and provide foundational data for the development of next-generation filters capable of preventing clogging in high-turbidity environments.

1. Introduction

Ballast water is a critical component of ship operations that ensures stability and structural integrity by adjusting a ship's draft. Typically, ballast water is transferred on board during cargo unloading at ports or nearby areas and is discharged at another port after the voyage. This can inadvertently facilitate the transfer of aquatic organisms, thus potentially adversely affecting aquatic ecosystems. Under a ballast-water capacity averaging one-third of a ship's volume, approximately 10 billion tons of water are transferred between aquatic ecosystems annually [1], along with more than 10,000 species of organisms daily [2].

To minimise aquatic environmental impact caused by the transfer of sea creatures via ballast water from ships, the International Maritime Organization (IMO) adopted a convention in 2004 to limit the maximum

---

[*] Corresponding author.

E-mail address: kjung@pusan.ac.kr

http://dx.doi.org/10.21278/brod76207

Received 26 December 2024; Received in revised form 14 February 2025; Accepted 19 March 2025

Available online 01 April 2025

ISSN 0007-215X; eISSN 1845-5859

numbers of viable organisms in discharged ballast water [3]. This convention, known as the International Convention for the Control and Management of Ships' Ballast Water and Sediment (BWMC), was implemented in 2017 to comply with a ballast-water performance standard (less than 10 viable organisms per cubic metre greater than or equal to 50 micrometres in minimum dimension and less than 10 viable organisms per millilitre less than 50 micrometres in minimum dimension and greater than or equal to 10 micrometres in minimum dimension; and discharge of the indicator microbes shall not exceed the specified concentrations), as specified in Regulation D-2. Moreover, ships on US routes have been required to comply with US Coast Guard (USCG) regulations for ballast water since 2012, which align with the IMO's BWMC D-2 standard [4]. Owing to these regulations, most ships operating in international ports are equipped with a type-approved ballast-water management system (BWMS).

A ship's ballast-water treatment technologies can be categorised into three types: physical, chemical, and other [5]. These methods are applied to ships using a combination of two different processes: pre-treatment and treatment. Pre-treatment, which occurs at the beginning of the major process in BWMSs, aims to remove large particles exceeding 50 μm in ballast water. Various types of filters are commonly used in BWMSs, including screen, hydrocyclone, bag, and self-cleaning filters, each employing a different filtration mechanism. The most commonly used method in pre-treatment is screen filtration [6], where the pore size ranges from 10 to 50 μm. Among the 46 BWMS types approved by the USCG, 36 utilise the filtration method [7]. Following filtration, the treatment process targets viable organisms in the ballast water to comply with the IMO's BWMC D-2 standard via chemical, physical, and biological methods.

One of the major issues with BWMSs is failure caused by water-quality problems, which is commonly referred to as 'clogging'. Clogging occurs when high concentrations of organic matter or sediment accumulate on filter elements, thereby obstructing water flow. This issue is exacerbated by the small pore sizes required for effective filtration, thus resulting in increased operational costs for filter cleaning and replacement [8] and reduced system efficiency [9-11]. Despite their critical impact, studies pertaining to clogging mechanisms, documented occurrences, and mitigation strategies are limited. Duan et al. [12] conducted a series of experiments on BWMS filters with varying pore sizes to investigate filtration efficiency. They showed that filtration efficiency increased as the pore size decreased; however, this improvement was accompanied by an increased risk of clogging. Jang et al. [13] conducted real-condition tests on various types of BWMSs using seawater with extremely high turbidity from the Shanghai Port in China. They reported that all filters with a mesh size of 50 μm used in the study failed due to clogging in severe turbidity conditions, thus highlighting the necessity of high-performance filters that can prevent clogging in environments with high particle concentrations in sea water. However, these studies primarily focused on experiments related to clogging phenomena and did not propose practical methods for application nor attempt to comprehensively investigate clogging mechanisms.

To mitigate the challenging issue of filter clogging, some researchers have focused on the development of advanced filters and the prediction of clogging in BWMSs. Sliwinski [14] proposed a machine-learning-based method to predict filter clogging in BWMSs. They leveraged operational data, including flow rates and pressure differentials, to develop a predictive model for the timely maintenance and optimisation of the treatment process. The proposed model achieved an accuracy exceeding 90 % using various neural network methods. Hyun et al. [15] proposed using a grinding device in a filtration system to achieve higher filtration efficiency under high-turbidity conditions. They evaluated the method via pilot and full-scale tests, which demonstrated 100 % efficiency for larger organisms exceeding 100 μm and 87–93 % for organisms smaller than 100 μm under high-turbidity conditions.

Despite the significant effect of filter clogging on ship operations, only a few studies have been conducted to address this issue. This is primarily attributed to the complex physical interactions within the filter and the inherent challenges of investigating these processes at the microscopic scale. To predict and prevent filter clogging, one must investigate the mechanisms underlying its occurrence and develop predictive analytical models for direct application in maritime operations. A comprehensive evaluation of filter performance based on a physical understanding of clogging is critical for devising effective strategies to mitigate clogging in BWMSs during ship operations.

Hence, this study is performed to predict the clogging occurrence time under varying marine environmental conditions and analyse the mechanisms of clogging in BWMS filters. This study examines particles in seawater, which are the primary cause of clogging, with emphasis on their composition, distribution, and concentrations in nearshore areas.

In this study, analytical methods capable of rapid computation are developed to evaluate the performance of screen filters in BWMSs by focusing on the complex phenomenon of filter clogging based on Darcy's law for porous media. To address the intricate hydrodynamic performance of ballast water within BWMS filters, computational fluid dynamics (CFD) simulations are conducted for the entire filter system, including the filter, basket, and backwash system. Furthermore, to investigate the mechanisms of filter clogging within fine pores, a coupled CFD-DEM (DEM = discrete-element method) is employed. This hybrid approach enables a detailed analysis of particle behaviour and fluid dynamics, thus offering insights unattainable via standalone methods, and has been used to capture localised and short-term behaviours. The findings of this study are expected to provide foundational data for predicting filter performance under clogging conditions in practical applications and contribute to the development of next-generation BWMS filters.

2. Investigation of solid-particle distribution characteristics in aquatic environment

Prior to examining the filter clogging of BWMSs, an investigation was conducted on solid particles in water that caused clogging on filters. The total solids contained in the water were classified based on their size and properties, as shown in Figure 1 [16]. First, total solids refer to suspended or dissolved matter and are classified into total dissolved solids (TDSs) smaller than 0.1 μm and total suspended solids (TSSs) larger than 0.1 μm. TSSs are classified into mineral matter (MM), which refers to inorganic materials such as silt, sand, and clay, and particulate organic matter (POM), which includes organic materials such as animal plankton. TDSs can be distinguished as mineral and dissolved organic matter depending on whether they are organic, similar to TSSs. This study focuses on TSSs, which significantly affect the filtration performance of BWMSs.

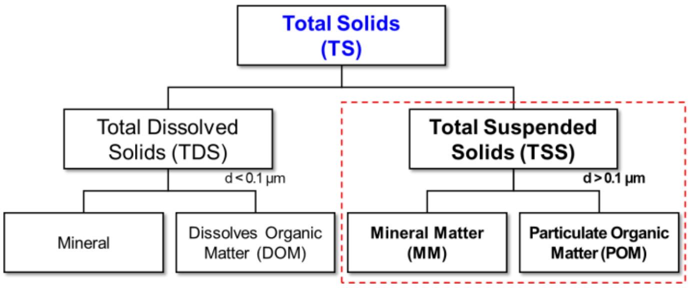

Fig. 1 Classification of particles in water

2.1 TSS

Table 1 summarises the reported TSS concentrations in various nearshore areas and major ports worldwide. The TSS concentration varied significantly by region, depending on the measurement date and precipitation at the time of measurement. The investigated TSS concentrations ranged from 15.7 to 300.1 mg/L on average, with the highest TSS concentration of 577.2 mg/L measured in the Yangtze River estuary in China. However, because this measurement does not include data from rainy periods, the TSS is expected to increase significantly. Extremely high TSS concentrations were measured in estuarine areas connected to the sea, primarily in the Yangtze River estuary in China, the Hodeidah port in Yemen, and the Gulf of Kambhat in India. Additionally, when particles accumulated on the seabed traverse to the water during rainfall, the TSS concentration can be higher compared with the case during non-rainy periods [17].

Table 1 List of TSS concentration ranges measured in nearshore areas

Measurement location (Country)	TSS concentration range (mg/L)	Measurement date (Period)	Precipitation	Reference
Yangtze River estuary (China)	23.2–577.2	Oct. 14–15, 2009 (2 days)	Excluded	[18]
Hodeidah port (Yemen)	10–440	Summer, 2001 3 months)	Included	[19]
Gulf of Kambhat (India)	94–312	2009–2010 (1 year)	Included	[20]
Semerang city (Indonesia)	40–160	Sep. 9, 2018 (1 day)	Excluded	[21]
Chennai port (India)	58–127	Dec. 2002–Mar. 2003 (3 months)	Excluded	[22]
Santos bay (South Africa)	12.3–83	2006–2007 (1 year)	Included	[23]
San Francisco bay (US)	30–80	May–Sep., 1996 (3 months)	Included	[24]
Atlantic coast (US)	60–75	2002 (1 year)	Included	[25]
Chesapeake bay (US)	5–70	May, Jul., Oct., 1996 (3 months)	Included	[26]
Ujung Genteng (Malaysia)	20–60	2000–2016 (17 years)	Included	[27]
Gulf of Mexico (US)	17–46	1989–1991 (3 years)	Included	[25]
Xuwen county (China)	5.8–37.8	Jan. 13–14, 2013 (2 days)	Excluded	[18]
Gulf of Suez (Egypt)	18.6–37.6	Every season, 2016	Included	[28]
Nak-dong river mouth (ROK)	2.9–28.5	2018–2021 (3 years)	Included	[29]

In the IMO G8 Guidelines for the approval of BWMSs as well as in the new IMO-type approval standard of BWMSs applicable from 28 October 2020 (BWMS Code, [30]), different operational criteria for TSS concentrations based on salinity levels are suggested, as presented in Table 2. In brackish regions, BWMS operation is tested under TSS concentrations of 50 mg/L or higher. The TSS levels specified in the IMO G8 Guidelines may be significantly lower than the actual TSS concentrations in the waters, thus indicating that even approved BWMSs can be affected by filter clogging during actual operations. To prevent clogging during ship operations, high-performance BWMS filters that can function under more severe conditions with higher TSS concentrations must be developed.

Table 2 Performance criteria of BWMS operation in various salinity range [31]

	Marine water (28–36 PSU)	Brackish water (10–20 PSU)	Fresh water (< 1 PSU)
Dissolved organic carbon	> 1 mg/L	> 5 mg/L	> 5 mg/L
Particulate organic carbon	> 1 mg/L	> 5 mg/L	> 5 mg/L
Total suspended solids	> 1 mg/L	> 50 mg/L	> 50 mg/L

2.2 MM

For the TSS in seawater, the MM, which represents inorganic matter, includes the following types of particles observed in the ballast tanks of ships [31]:

- Clay: Particles measuring 2 μm or less, typically dominated by silicate minerals with traces of metal oxides and organic matter.
- Silt: Particles measuring 263 μm, primarily composed of quartz and feldspars.
- Sand: Particles measuring 63 µm to 2 mm, comprising either quartz or calcium carbonate.
- Larger soil particles: Particles exceeding 2 mm, primarily gravel.

Figure 2 shows the composition ratio of MM in nearshore areas, as reported in the literature [32-37]. The composition of MM varies slightly depending on the region but primarily comprises fine particles measuring less than 63 µm known as mud, which is a mixture of clay and silt. This implies that when employing a filter with a pore size of 10–50 µm primarily for pre-treatment in BWMSs, filter clogging can occur frequently.

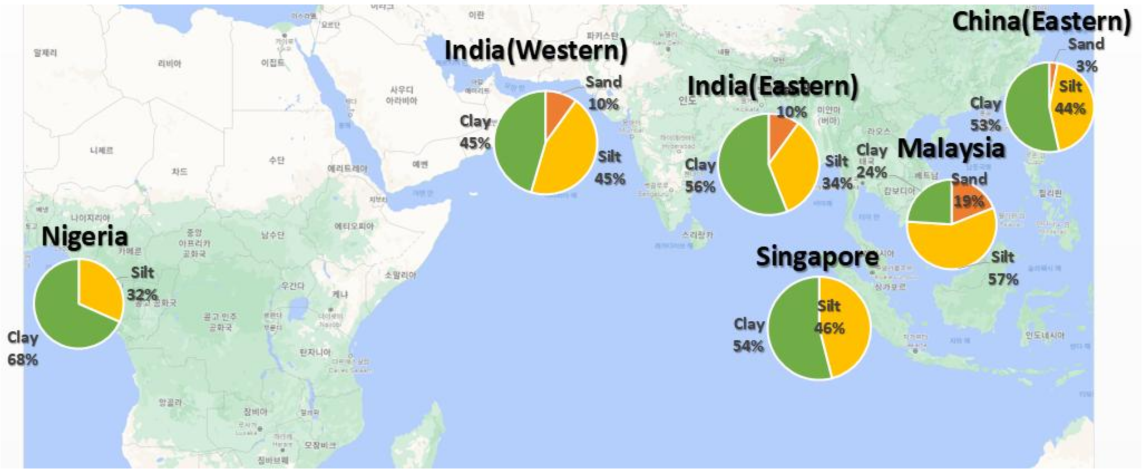

Fig. 2 Mineral-matter distributions measured in various nearshore areas

2.3 POM

POM, which represents particulate organic matter in seawater, is primarily measured based on carbon and is also expressed as particulate organic carbon (POC). The POC concentration in aquatic environments worldwide is 0–0.3 mg/L [38], which corresponds to less than 0.1 % of the TSS concentration in areas with a TSS concentration of 300 mg/L. In other words, POM constitutes a minute portion of the TSS and thus is expected to minimally affect filter clogging. The POC may differ depending on the region; nonetheless, it fluctuates by 0 to 0.2 mg/L depending on the seasons [39] and by only 0 to 3.0 mg/L depending on the precipitation amount [40]. In other words, POM constitutes a minute portion of the TSS and thus is expected to minimally affect filter clogging. The TSS in aquatic environments is primarily composed of MM, and among them, small inorganic particles, such as clay and silt, are major contributors to filter clogging.

3. Mathematical background

This section provides a mathematical overview of two methods for evaluating the performance of ship BWMS filters: the analytical method and CFD simulations. Additionally, it introduces the CFD-DEM approach for estimating clogging mechanisms at the microscale in localised filter regions.

3.1 Analytical methods

In the design and operation of BWMS filters, pressure drop due to the filter screen is a crucial factor. The pressure drop (ΔP_{total}) caused by the filter system can be classified into the pressure drop caused by fluid passing through the filter screen (ΔP_{screen}) and the pressure drop caused by the accumulation of substances, known as the 'filter cake' (ΔP_{cake}), on the filter, as shown in Equation (1):

$$\Delta P_{total} = \Delta P_{screen} + \Delta P_{cake} \tag{1}$$

In this study, Darcy's law [41], which describes the relationship between velocity and pressure drop in porous media, was used to estimate the pressure drop caused by the screen and filter cake. Darcy's equation for estimating pressure drop by the screen (ΔP_{screen}) is shown in Equation (2):

$$\Delta P_{screen} = \frac{1}{A}\frac{1}{B}\frac{\mathrm{d}V}{\mathrm{d}t}\mu T \tag{2}$$

where A is the screen area, V the volume of fluid passing through the BWMS, t the time, B the specific permeability of the screen, μ the viscosity coefficient of the fluid, and T the screen thickness. The screen permeability (B) can be estimated using the Kozeny–Carman equation [5], which relates B to the geometry of the screen, as shown in Equation (3):

$$B = \frac{1}{K_0 S_0^2}\frac{\varepsilon^3}{(1-\varepsilon)^2} \tag{3}$$

where ε is the porosity of the screen; K_0 is the Kozeny coefficient, which can be obtained using Equation (4); and S_0 is the specific surface area of the screen, which can be obtained using Equation (5):

$$K_0 = \frac{4\varepsilon^3}{(1-\varepsilon)^{0.5}}[1 + 56(1-\varepsilon)^3] \tag{4}$$

$$S_0 = \frac{\pi d}{\pi (d/2)^2} \tag{5}$$

where d is the equivalent cylinder diameter of the screen [5]:

$$d = \sqrt{\frac{Q}{1.8\varepsilon\pi}} \tag{6}$$

Here, Q denotes the filter design flow rate. Subsequently, the pressure drop of the filter screen can be derived as follows:

$$\Delta P_{screen} = \frac{64u\mu T}{d^2}(1-\varepsilon)^{1.5}[1 + 56(1-\varepsilon)^3] \tag{7}$$

where u denotes the filtration velocity. The pressure drop caused by the filter cake (ΔP_{cake}) can be estimated using Darcy’s equation for porous media, as shown in Equation (8):

$$\Delta P_{cake} = \frac{\mu r l}{A}\frac{\mathrm{d}V}{\mathrm{d}t} \tag{8}$$

where l is the filter-cake thickness and r is the transmission coefficient, which can be obtained using Equation (9):

$$r = \frac{5(1-e)^2 S^2}{e^3} \tag{9}$$

Here, e is the average porosity of the filter cake and S is the specific area of the particles, which can be calculated via Eq. (5) using the particle diameter: The filter-cake thickness can be determined by calculating the volume of the filter cake per unit volume [42] using Equation (10):

$$v = \frac{lA}{V} \approx \frac{\rho_f J}{(1-J)(1-e)\rho_s - J e \rho_f} \tag{10}$$

where ρ_f and ρ_s are the densities of the fluid and solid, respectively; and J is the mass fraction of solid in the fluid. Subsequently, Equation (8) can be expressed as follows:

$$\Delta P_{cake} = \frac{5(1-e)^2 S^2 \mu v V^2}{e^3 A^2 t} \tag{11}$$

Finally, the total pressure drop of the filter screen can be expressed analytically using Equation (12), by summing Equations (7) and (11):

$$\Delta P_{total} = \frac{64u\mu T}{d^2}(1-\varepsilon)^{1.5}[1 + 56(1-\varepsilon)^3] + \frac{5(1-e)^2 S^2 \mu v V^2}{e^3 A^2 t} \tag{12}$$

In this study, the performance of the backwash system, which is primarily used in BWMS filters to prevent screen clogging, was predicted. When using the suction nozzle for backwashing in the filter, some of the water flowing into the BWMS is discharged owing to suction, and the loss flow rate (Q_{loss}) can be calculated by multiplying the area of the suction nozzle tip (A_{nozzle}) by the suction speed at the nozzle tip (u_{nozzle})), as shown in Equation (13):

$$Q_{loss} = u_{nozzle} * A_{nozzle} \tag{13}$$

u_{nozzle} can be estimated using the Bernoulli equation as follows:

$$u_{nozzle} = \sqrt{\frac{2}{\rho_f}\Delta P_{nozzle}} \tag{14}$$

where ΔP_{nozzle} is the pressure drop at the tip of the suction nozzle.

3.2 CFD simulations

CFD simulations were performed in this study to analyse the localised clogging mechanism of the BWMS filter at the microscale. The Reynolds averaged Navier-Stokes (RANS) equation was employed using the commercial CFD software STAR-CCM+ v13.06 [43] for an incompressible, steady, single-phase flow (liquid) under isothermal conditions by incorporating the continuity equation:

$$\frac{\partial(\rho\overline{u_i})}{\partial t}+\frac{\partial}{\partial x_j}(\rho\overline{u_i u_j})=-\frac{\partial\bar{p}}{\partial x_i}+\frac{\partial\overline{\tau_{ij}}}{\partial x_j}+\frac{\partial}{\partial x_j}(-\rho\overline{u'_i u'_j}) \tag{15}$$

$$\frac{\partial(\rho\overline{u_i})}{\partial x_i}=0 \tag{16}$$

where ρ is the density, $\overline{u_i}$ is the relative averaged velocity vector for the flow between the fluid and the control volume, $\overline{u_i u_j}$is the Reynolds stress, x_i is the coordinate, $\bar{p}$ is the mean pressure, and $\overline{\tau_{ij}}$is the mean shear stress tensor which can be expressed as:

$$\overline{\tau_{ij}}=\mu\left(\frac{\partial\overline{u_i}}{\partial x_j}+\frac{\partial\overline{u_j}}{\partial x_i}\right) \tag{17}$$

where μ is the dynamic viscosity.

The equations were solved using second-order numerical methods for both time and space discretisation. In the simulation, the semi-implicit method for pressure-linked equations was used to couple the velocity and pressure. Additionally, the standard k-ω turbulence model was used owing to its suitability for rotational flows.

The filter screen, i.e. the focus of the CFD analysis, contains a porous layer with extremely small pores, which complicates the modelling and numerical analysis. Therefore, the pressure drop across the screen was analysed for different incoming flow velocities via a series of numerical simulations.

The resistance force (f_p) of the porous medium is defined in terms of the velocity V and porous resistance tensor P, as shown in Equation (18) [43]:

$$f_p=-P\cdot V \tag{18}$$

The porous resistance tensor P comprises two components, as shown in Equation (19):

$$P=P_V+P_I|V|, \tag{19}$$

where P_V and P_I represent the viscous and inertial resistance coefficients, respectively. These coefficients were derived from numerical experiments and are explained in detail in Section 5.2.

In this study, the DEM was used to analyse clogging occurrences on a localised filter screen at the microscale under severe TSS conditions. CFD-DEM is a method for analysing the multiphase flow of fluids and particles by combining the Eulerian methodology for fluids and the Lagrangian methodology for particles. Unlike CFD, which analyses fluids, the DEM focuses on the motion and interaction of individual particles based on Newton’s law of motion and contact mechanisms [44]. The particle dynamics were calculated using the classic momentum conservation equations and a particle-index representation as follows [43]:

$$m_i\frac{\mathrm{d}v_i}{\mathrm{d}t}=m_i g+\sum F_{cont}+F_{drag}+F_{pres}+F_{added} \tag{20}$$

$$I_i\frac{\mathrm{d}\omega_i}{\mathrm{d}t}=\sum M_{cont}+M_{drag} \tag{21}$$

where subscript i represents the particle number; F_{cont} and M_{cont} are the forces and moments due to contact, respectively; $F_{drag,}$ F_{pres}, and F_{added} are the hydrodynamic forces of drag, pressure gradient, and added mass terms, respectively; and M_{drag} is the torque resulting from fluid interaction. In this study, the contact dynamics between the particles were modeled as one-way coupling from the fluid to particle, thus ensuring that the particles do not affect the fluid dynamics.

4. Test model and conditions

In this study, a basket-type filter system (with a processing capacity of approximately 300 tons/h), which is widely used as pretreatment for BWMSs owing to its simple design. A plain-weave screen with a pore size of 40 μm was selected for the filter screen, and the main specifications of the basket and the screen considered in this study are shown in Table 3.

Table 3 Principal dimensions of basket-type filter and screen

Component	Parameter	Value
Basket	Basket outer diameter	620 mm
	Basket inner diameter	585 mm
	Inlet, outlet pipe diameter	220 mm
Screen	Screen inner diameter	440 mm
	Screen height	830 mm
	Thickness (T)	0.25 mm
	Porosity (ε)	0.146

This filter was assumed to operate in an environment with a high concentration of TSS (i.e. 1,000 mg/L). Clogging is considered to have occurred when the pressure drop of the filter system reaches 0.5 bar due to particles during operation [13]. Additionally, the pressure at the filtration outlet was maintained at 3 bar.

Furthermore, a backwash system with suction nozzles was used for the basket-type filter, as shown in Figure 3. The suction nozzle comprises four nozzle tips with a length and width of 0.18 and 0.005 m, respectively. The backwash system was assumed to be operating under a continuous rotation at 170 RPM during the BWMS filter operation. Considering a 10 % loss of flow entering the BWMS due to the backwash system, the flow velocity and pressure drop at the suction nozzle tip can be analytically estimated as 2.08 m/s and 0.0217 bar, respectively, using Equations (13) and (14), respectively.

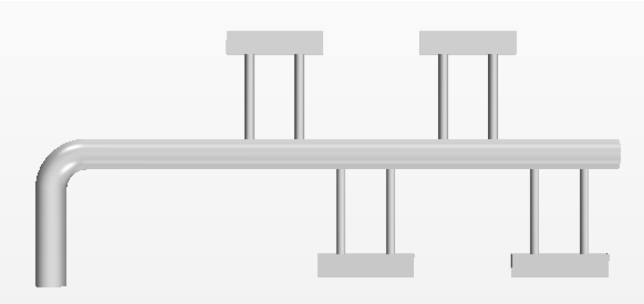

Fig. 3 Model of backwash suction nozzle

5. Results and discussions

5.1 Performance evaluation of filter screen via analytic analysis

Figure 4 presents the estimated pressure drop and filter-cake thickness over time for a BWMS filter with a plain-weave screen designed for a capacity of 300 tons/h, operating at a TSS concentration of 1,000 mg/L without incorporating a backwash system. For the analysis, all particles in the water were assumed to measure 50 μm. As shown in Figure 4(a), the initial pressure drop across the screen was approximately 0.059 bar when the system began to operate. During the BWMS operation, the pressure drop increased steadily at a rapid rate of approximately 0.688 bar/h, where 0.5 bar was attained in merely 42.6 min, thus indicating the onset of clogging in the filter system. As illustrated in Figure 4(b), the filter-cake thickness was approximately

10.34 mm, which corresponds to approximately 5 % of the cylindrical-screen radius. These findings indicate that under high-turbidity conditions of 1,000 mg/L, clogging can develop within less than 1 h of operation.

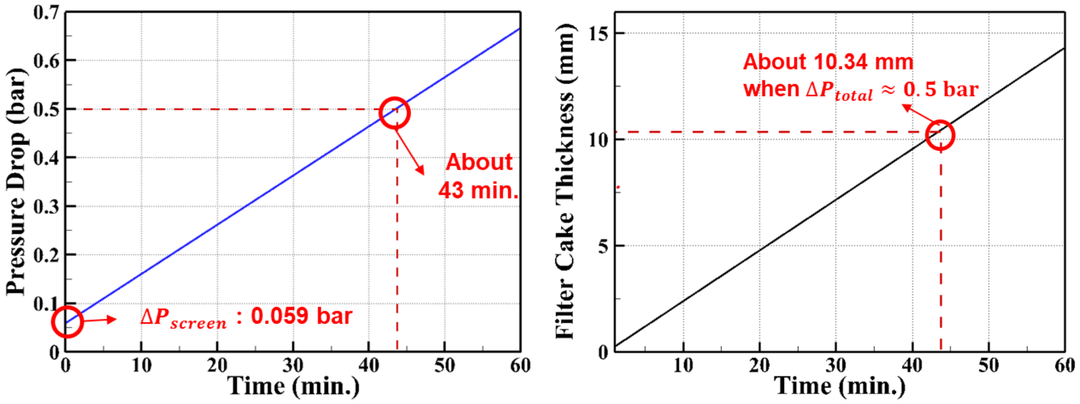

(a) Clogging time (b) Filter-cake thickness

Fig. 4 Estimation of clogging time and filter-cake thickness using analytic method

Figure 5 presents the analysis of the time to clogging of the screen under varying TSS concentrations and particle sizes. As shown in Figure 5(a), the time to clogging decreased exponentially as the TSS concentrations with a uniform particle size of 50 µm increased. Specifically, at 50 mg/L, which complies with the IMO G8 Guideline [45], clogging occurred after approximately 860.1 min, whereas at 500 mg/L, i.e. the maximum TSS concentration in the Yangtze River estuary, clogging occurred in approximately 85.8 min. Considering that typical ballasting operations may require 24 h [46], the system is expected to operate without clogging at TSS levels of up to 30 mg/L. Additionally, Figure 5(b) illustrates the effect of particle-size variations, showing that as the particle size increased, both the time to clogging and the corresponding filter cake thickness exhibited a quadratic relationship.

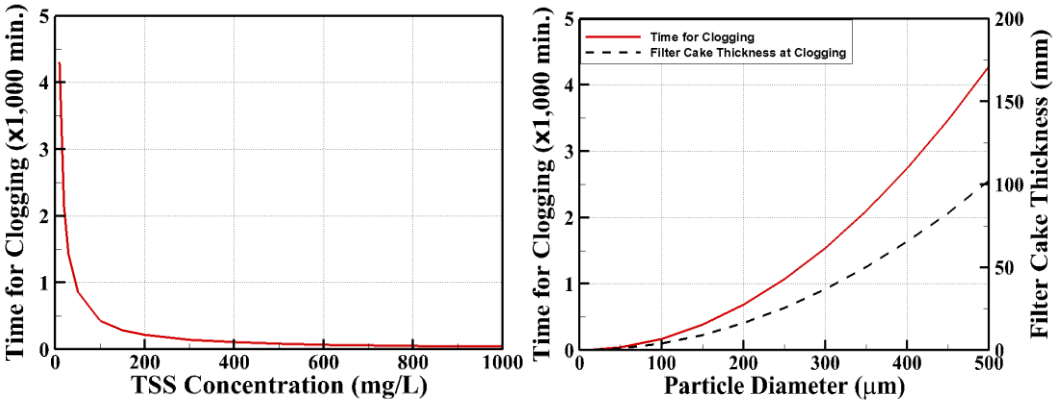

(a) TSS concentration (b) Particle diameter

Fig. 5 Estimation of clogging time with varying TSS concentration and particle diameter

5.2 Performance evaluation of filter screen using CFD

5.2.1. Estimation of pressure drop for local screen

Before estimating and analysing the performance of the filter using CFD, numerical experiments were performed on a local screen to numerically model the plain weave screen geometry in CFD and estimate the inertia and viscous resistance coefficients, P_I and P_V, in Equation (19). The numerical experiments involved varying the flow rate and screen size to analyse their effects on the P_I and P_V, as summarised in Table 3. The shape and mesh structure of the screen model are shown in Figure 6.

Table 3 Test cases for estimation of P_I and P_V for local screen

Case no.	Screen size (mm^2)	Num. of cells	Velocity (m/s)
1	0.84 × 1.00	0.43×10^6	0.055 0.100 0.200 0.300 0.400
2	1.69 × 2.00	1.70×10^6	
3	3.38 × 4.00	8.30×10^6	

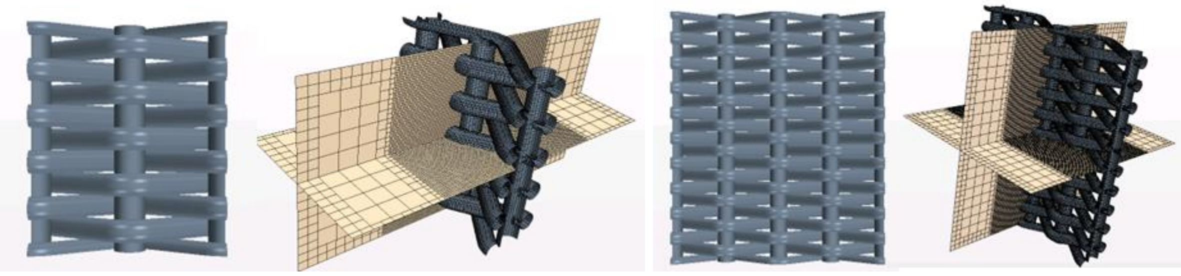

(a) Case 1 (b) Case 2

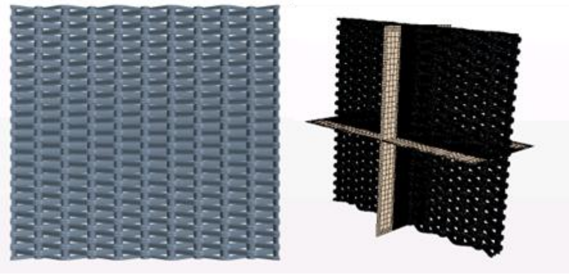

(c) Case 3

Fig. 6 Test model and mesh structure for estimation of P_I and P_V for local screen

Figure 7 shows the pressure and velocity fields on the plain-weave screen analysed using CFD simulations at a flow velocity of 0.4 m/s. A region of relatively high pressure developed on the upstream surface where the fluid entered, leading to localised acceleration as the fluid passed through the pores of the screen. The variations in the pressure drop with respect to screen size and flow velocity are shown in Figure 8. This numerical experiment confirmed that the screen size does not affect the pressure drop, whereas the pressure drop increases quadratically with the flow velocity. Based on this, the screen size required to estimate the P_I and P_V can be determined. The estimated P_I and P_V, corresponding to changes in the flow velocity were 6.57×10^6 and 2.42×10^7, respectively.

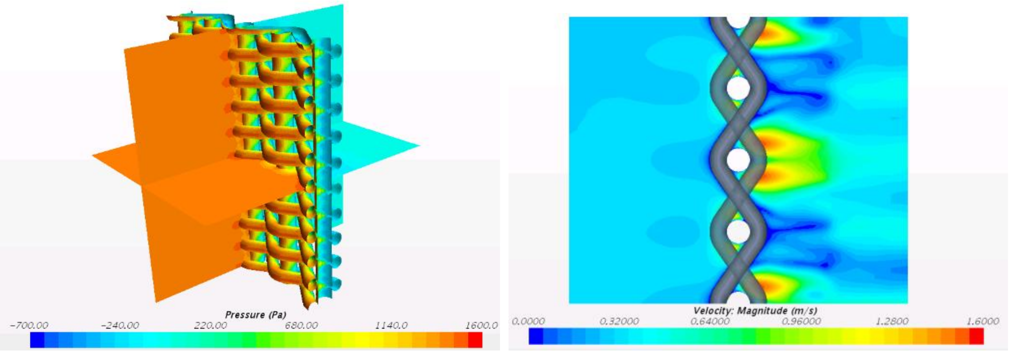

(a) Pressure field (b) Velocity field

Fig. 7 Pressure and velocity fields of local screen (Case 2)

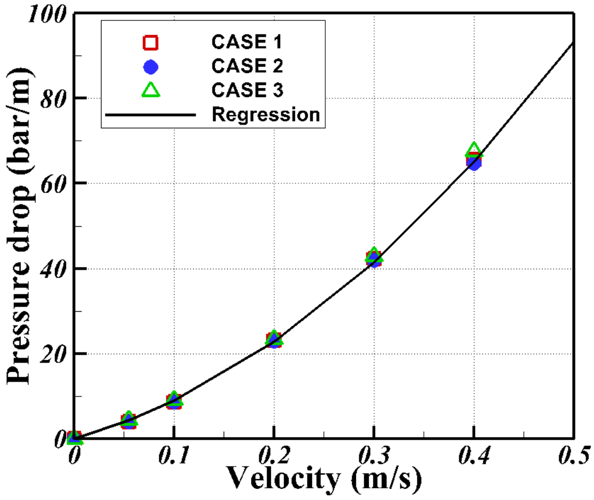

Fig. 8 Pressure-drop estimation results of local screen for varying screen size and flow velocity

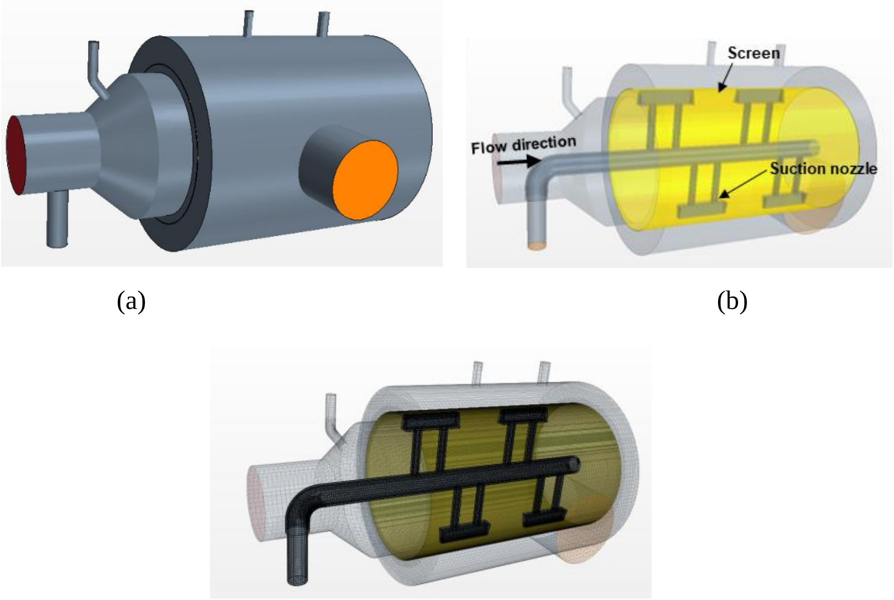

(a)

(b)

(c)

Fig. 9 Test model and mesh structure of filter system in BWMS

5.2.2. Performance evaluation of BWMS filter with backwash system

The hydrodynamic performance of the BWMS filter, including the backwash speed at the nozzle and pressure drop for the entire filter system with a basket, was assessed via CFD simulations. The screen was modelled as a virtual porous medium instead of modelling it using the P_I and P_V obtained from the numerical experiments for the filter screen. The key components of the BWMS, such as the screen, suction nozzle system for the backwash, and basket, were numerically modelled, as shown in Figure 9. The total number of grids used in the modelling was 2.1 million (Figure 9 (c)).

Figure 10 shows the pressure and velocity fields as well as the streamlines obtained from the CFD simulation of the filter without backwash operation. The fluid entering the filter exhibited a significant rotational flow as it flowed upwards inside the screen before losing velocity upon reaching the bottom surface and ultimately passing through the screen (Figure 10 (c)). The simulation results indicated that the fluid experienced a pressure drop while passing through the screen (Figure 10 (a)). In the basket, the flow velocity decreased upon entry but increased again at the outlet after passing through the screen (Figure 10 (b)). The pressure drop across the screen, estimated via CFD simulation, was approximately 0.091 bar, which was approximately 35 % higher than that estimated using the analytical method (0.059 bar). This discrepancy can be attributed to additional factors considered in the CFD simulation, such as the geometry of the suction nozzle, the positions of the basket inlet and outlet, and the effects of gravity, which were not considered in the analytical method.

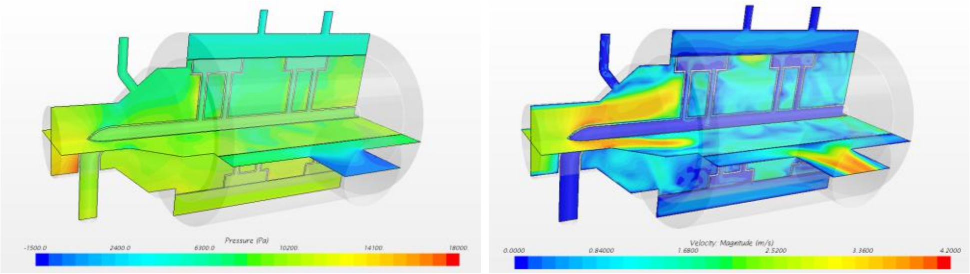

(a) Pressure field (b) Velocity field

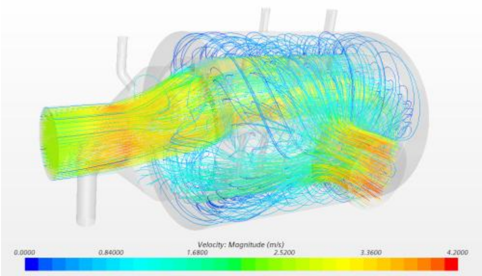

(c) Streamline

Fig. 10 Pressure and velocity fields, and streamline of filter system in BWMS without backwash operation

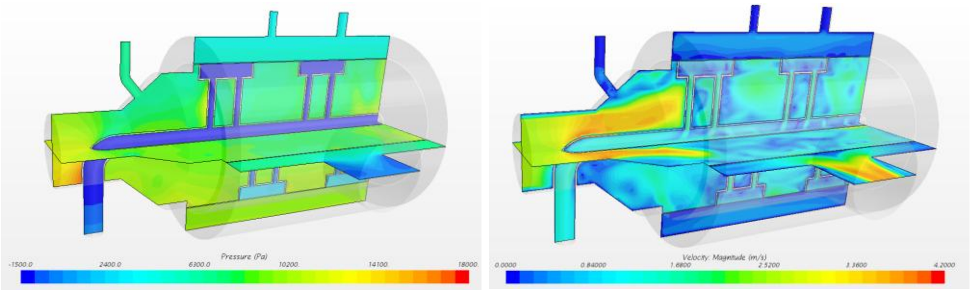

(a) Pressure field (b) Velocity field

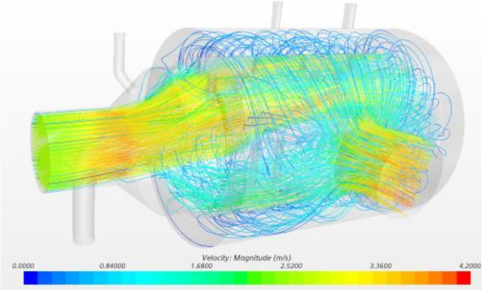

(c) Streamline

Fig. 11 Pressure and velocity fields, and streamline of filter system in BWMS with backwash operation

The CFD simulation results for the BWMS filter with the backwash system operating via the suction nozzle (Figure 3) are shown in Figures 11 and 12. As shown in Figure 11, the overall pressure and velocity fields as well as the streamline patterns were similar to those observed prior to the activation of the backwash system (Figure 10). However, during the backwash operation, a region of relatively low pressure developed at the tip of the suction nozzle, causing the fluid to pass from the screen surface into the nozzle, as illustrated in Figure 12(a). The velocity at the suction nozzle tip was estimated to be approximately 2.01 m/s, which is almost identical to the analytically calculated value of 2.08 m/s. Additionally, the pressure drop induced by the suction nozzle, as estimated via CFD simulation, was approximately 0.020 bar, whereas it was estimated to be 0.022 bar via the analytical method (Equation (14)). These results demonstrate that the analytical method provides performance estimates for the suction nozzle that were almost identical to the results obtained from the CFD simulation.

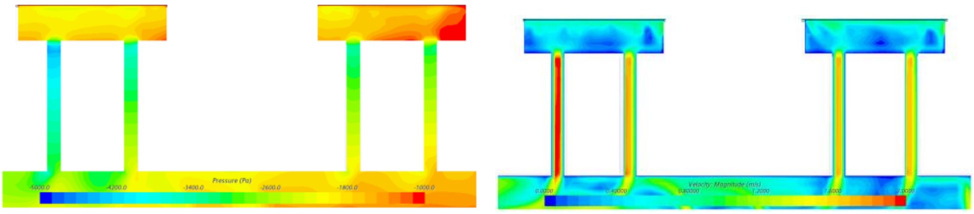

(a) Pressure field (b) Velocity field

Fig. 12 Pressure and velocity fields of backwash suction nozzle

5.2.3. Investigation of clogging-occurrence mechanism using CFD-DEM

The clogging mechanism of a local screen was analysed at the microscale via CFD-DEM simulations. The screen used in this study measured 1.69 mm × 2.00 mm, as specified in Case 2 of Table 3. Simulations were performed at a TSS concentration of 1,000 mg/L. The DEM analysis was performed under particle sizes ranging from 20 to 70 µm, a screen pore size of 40 µm, and the assumption of spherical particles.

Figure 13 shows images of particle accumulation on the local screen surface. Approximately 0.1 s after the fluid began to flow through the screen (Figure 13 (b)), particles larger than 70 μm, which exceeded the screen pore size, began to obstruct some of the pores. By 0.5 s (Figure 13(c)), particle accumulation localised around the pores obstructed by relatively larger particles. Eventually, within 1 s of fluid-flow initiation, the particles almost occupied the entire screen surface. This indicates that clogging on the filter screen began at locations where relatively large particles were obstructed by the screen. Once an obstruction occurs, a large area of the screen becomes rapidly occupied by particles. These findings highlight the importance of managing relatively large particles to prevent filter clogging.

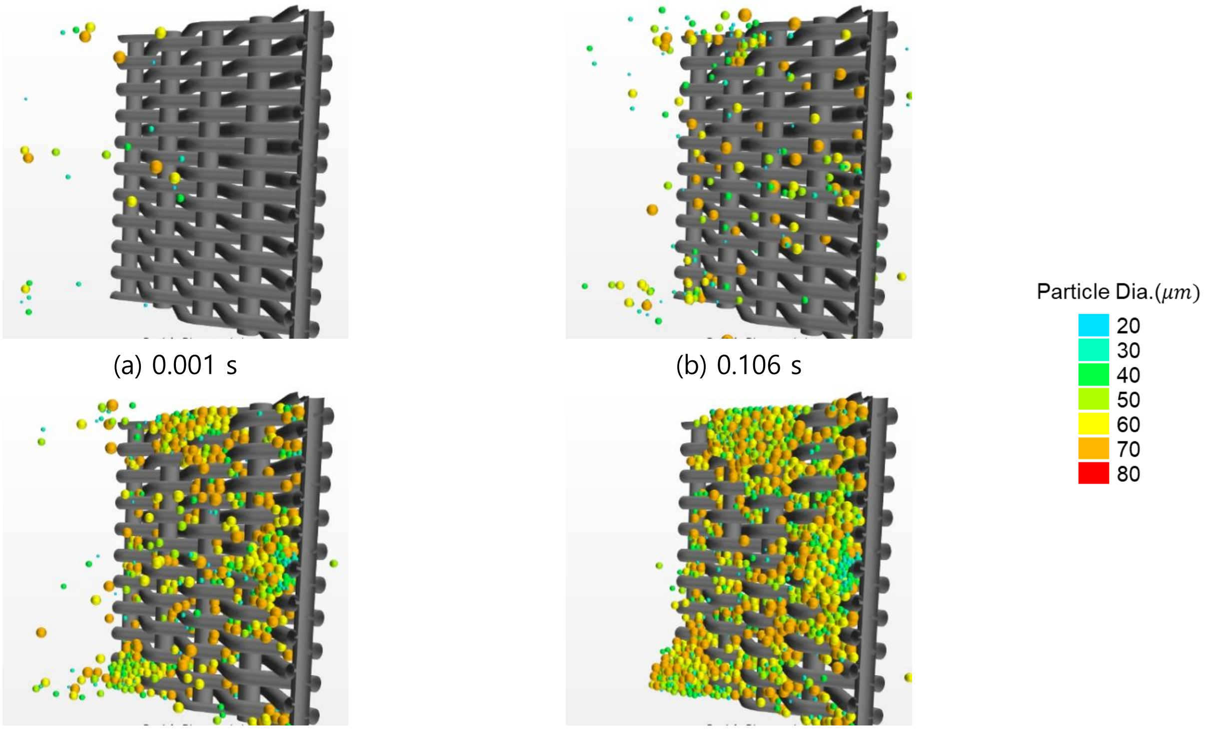

(a) 0.001 s (b) 0.106 s

(c) 0.511 s (d) 1.040 s

Fig. 13 Images of clogging generation on local screen via CFD-DEM simulation

Figure 14 shows a comparison of the velocity distribution around the screen in the presence and absence of particles. When particles accumulated on the screen (Figure 14(b)), unlike the case without particles, a localised increase in velocity was observed, which potentially exerted greater loads on the screen. The time-dependent pressure drop resulting from particle accumulation is shown in Figure 15. The pressure drop increased by 0.02×10^{-3} bar within 1 s, and assuming a linear increase over time, the pressure drop is estimated to reach the clogging threshold of 0.5 bar after approximately 41.7 min. This prediction aligns closely with the clogging time of 42.6 min estimated using the analytical method, thus confirming its consistency.

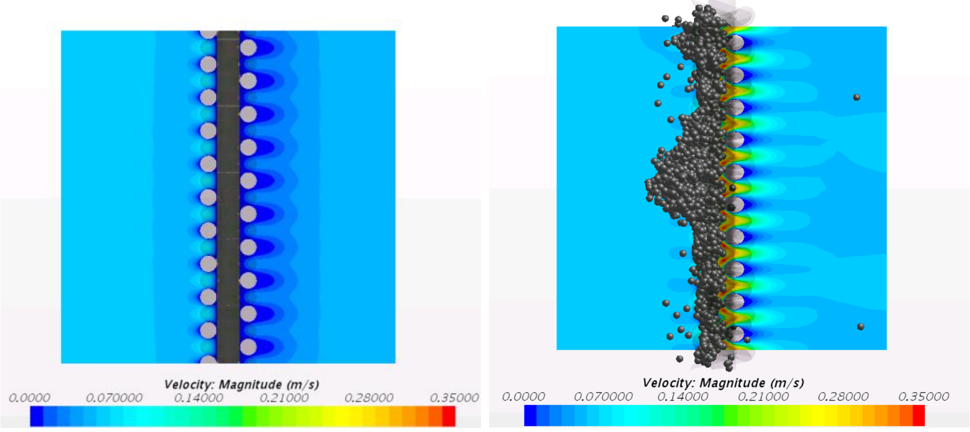

(a) without particles (b) with particles

Fig. 14 Comparison of velocity fields around local screen between cases with and without particles at t = 0.104 s

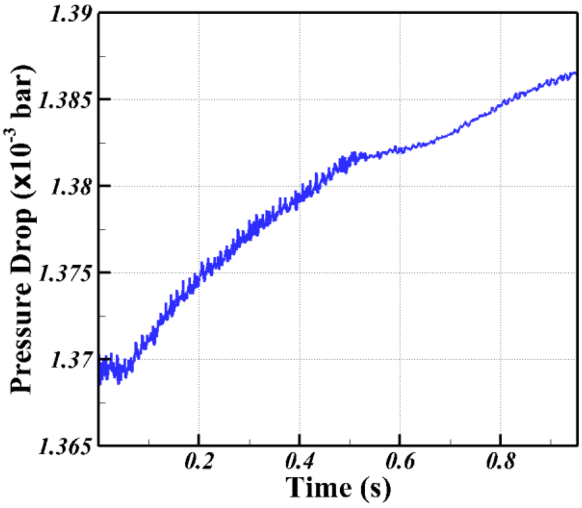

Fig. 15 Pressure-drop results of local screen estimated using CFD-DEM method

6. Conclusions

This study investigated filter clogging mechanisms in a BWMS by integrating analytical modelling and CFD-DEM simulations. The results indicated that clogging occurred rapidly under high-TSS conditions, and that the clogging time, pressure drop, and filter-cake thickness predicted by the analytical model aligned well with the results of CFD simulations. The DEM approach provided further insights into the microscopic clogging process, thus revealing the manner by which particles accumulated on the filter screen and interacted with the backwash system. These findings contribute to the optimisation of the BWMS filter performance and improvements to clogging-mitigation strategies.

The key findings in this study are listed below:

- Particles in seawater are primarily composed of inorganic matter, particularly small clay and silt particles. The actual TSS concentrations in the water may be significantly higher than the IMO G8 Guidelines, which implies that even BMWSs with type approval can be affected by filter clogging

during their operations. From a shipowner's perspective, frequent clogging may increase maintenance costs, extend ballast-water treatment times, and require higher energy consumption owing to increased pump pressure.
- An analytical method based on Darcy's law was proposed to assess the performance of the filter screens by considering the effect of the filter cake. The results yielded by the method for the pressure drop of the filter screen and filter cake, the flow speed and pressure drop at the suction nozzle tip, and the clogging time agreed well with the results of CFD simulations for the entire BWMS filter with backwash operation.
- The clogging mechanism on a plain-weave screen was investigated via CFD-DEM simulations. The results showed that particles larger than the pores first began obstructing the screen pores, whereas other particles began to accumulate on the screen and occupied the entire screen rapidly. The clogging time estimated by the CFD-DEM simulations agreed well with the results yielded by the analytical method and CFD simulations.

The analytical method proposed herein for evaluating the filter performance BWMSs presents certain limitations as it does not consider the specific device configurations, such as the different filter types and backwash systems. Nevertheless, it provides rapid estimates with low computational loads, particularly under severe ballast conditions and high TSS levels. This method, along with the CFD analysis techniques developed in this study, is expected to be applicable for predicting the filter-clogging performance of BWMSs in diverse ocean environments, where complex physical phenomena contribute to clogging. Furthermore, these approaches, combined with insights into clogging mechanisms obtained through CFD-DEM analysis from a microscopic perspective, are expected to serve as foundational data for the development of next-generation BWMS filters designed to prevent clogging in advance.

ACKNOWLEDGEMENT

This work was supported by the National Research Foundation of Korea (NRF) funded by the Ministry of Science and ICT (MSIT) (RS-2024-00405278), and New Renewable Energy Core Technology Development Project (RS-2024-00450063) funded by the Ministry of Trade, Industry and Energy.

REFERENCES

[1] International Maritime Organization, 2000. GloBallast programme. *London: Ballast Water News*, 1, 2–3.

[2] Carlton, J. T., 1999. The scale and ecological consequences of biological invasions in the world's oceans. *Kluwer Academic Publishers*. 195-212. https://doi.org/10.1007/978-94-011-4523-7_13

[3] International Maritime Organization, 2004. International Convention for the Control and Management of Ship's Ballast Water and Sediment.

[4] US Environmental Protection Agency. Generic Protocol for the Verification of Ballast Water Treatment Technology (EPA/600/R-10/146). 2010.

[5] Chen, N., Yang, Z., Luo, W., 2021. Development and implementation of ship BWMS. *Springer*. https://doi.org/10.1007/978-981-33-6865-1

[6] Yilmaz, M., Bilgin Güney, C., 2023. Evaluation of ballast water treatment systems from the perspective of expert seafarers' ship experiences. *Brodogradnja*, 74(4), 129-154. https://doi.org/10.21278/brod74407

[7] USCG, 2021. BWMS type approval status. https://www.dco.uscg.mil/msc/ballast-water/TACs/ (Accessed Feb. 11, 2024).

[8] American Bureau of Shipping, 2019. Best Practices for Operations of Ballast Water Management Systems Report.

[9] Tsolaki, E., Diamadopoulos, E., 2010. Technologies for ballast water treatment: a review. *Journal of Chemical Technology & Biotechnology*, 85(1), 19-32. https://doi.org/10.1002/jctb.2276

[10] Yonsel, F., Vural, G., 2017. KPI (key performance indicators) application on ballast water treatment system selection. *Brodogradnja*, 68(3), 67-84. https://doi.org/10.21278/brod68305

[11] Bilgin Güney, C., Danişman, D. B., Ertürk Bozkurtoğlu, Ş. N., Yonsel, F., 2018. Determination of sediment accumulation pattern in A double bottom ballast tank model. *Brodogradnja*, 69(2), 55-67. https://doi.org/10.21278/brod69204

[12] Duan, D., Xu, F., Wang, T., Guo, Y., Fu, H., 2023. The effect of filtration and electrolysis on ballast water treatment. *Ocean Engineering*, 268, 113301. https://doi.org/10.1016/j.oceaneng.2022.113301

[13] Jang, P. G., Hyun, B., Shin, K., 2020. Ballast water treatment performance evaluation under real changing conditions. *Journal of Marine Science and Engineering*, 8(10), 817. https://doi.org/10.3390/jmse8100817

[14] Sliwinski, K., 2019. A machine learning approach to predictively determine filter clogging in a ballast water treatment system. Master Thesis, *School of Industrial Engineering and Management*, Stockholm, Sweden.

[15] Hyun, B., Cha, H. G., An, Y. K., Park, Y. S., Jang, M. C., Jang, P. G., Shin, K., 2021. Potential applications of a novel ballast water pretreatment device: grinding device. *Journal of Marine Science and Engineering*, 9(11), 1213. https://doi.org/10.3390/jmse9111213

[16] Woodard, F., 2001. Industrial waste treatment handbook. *Elsevier*.

[17] Weston, D. P., Moschet, C., Young, T. M., Johanif, N., Poynton, H. C., Major, K. M., Hasenbein, S., 2019. Chemical and toxicological effects on Cache Slough after storm-driven contaminant inputs. *San Francisco Estuary and Watershed Science*, 17(3). https://doi.org/10.15447/sfews.2019v17iss3art3

[18] Chen, S., Han, L., Chen, X., Li, D., Sun, L., Li, Y., 2015. Estimating wide range Total Suspended Solids concentrations from MODIS 250-m imageries: An improved method. *ISPRS Journal of Photogrammetry and Remote Sensing*, 99, 58-69. https://doi.org/10.1016/j.isprsjprs.2014.10.006

[19] Heba, H. M., Al-Edresi, M. A., Al-Saad, H. T., Abdelmoneim, M. A., 2004. Background levels of heavy metals in dissolved, particulate phases of water and sediment of Al-Hodeidah Red Sea coast of Yemen. *Marine Sciences*, 15(1). https://doi.org/10.4197/mar.15-1.3

[20] Misra, A., Murali, R. M., Sukumaran, S., Vethamony, P., 2014. Seasonal variations of total suspended matter (TSM) in the Gulf of Khambhat, west coast of India. *International Journal of Geo-Marine Sciences*, 43(7), 1202-1209.

[21] Sanjoto, T. B., Elwafa, A. H., Tjahjono, H., Sidiq, W. A. B. N., 2020. Study of total suspended solid concentration based on Doxaran algorithm using Landsat 8 image in coastal water between Bodri River estuary up to east flood canal Semarang City. *In IOP Conference Series: Earth and Environmental Science*, 561(1), 012053. https://doi.org/10.1088/1755-1315/561/1/012053

[22] Natesan, U., Kalaivani, S., 2007. Water Quality in and Around Chennai Port During Post Monsoon. *Pollution Research*, 26(4), 607.

[23] Giannini, M. F. C., Harari, J., Ciotti, A. M., 2017. The use of CBERS (China-Brazil Earth Resources Satellite) to trace the dynamics of total suspended matter at an urbanized coastal area. *Brazilian Journal of Oceanography*, 65(2), 309-323. https://doi.org/10.1590/s1679-87592017135006502

[24] Roman, M. R., Holliday, D. V., Sanford, L. P., 2001. Temporal and spatial patterns of zooplankton in the Chesapeake Bay turbidity maximum. *Marine Ecology Progress Series*, 213, 215-227. https://doi.org/10.3354/meps213215

[25] Baskaran, M., Coleman, C. H., Santschi, P. H., 1993. Atmospheric depositional fluxes of 7Be and 210Pb at Galveston and College Station, Texas. *Journal of Geophysical Research: Atmospheres*, 98(D11), 20555-20571. https://doi.org/10.1029/93JD02182

[26] Baldizar, J. M., Rybicki, N. B., 2006. Primary factors affecting water clarity at shallow water sites throughout the Chesapeake and Maryland coastal bays. *In Proceedings of the 8th Federal Interagency Sedimentation Conference*, 2-6 April, Reno, NV, USA.

[27] Ditriyani, E., Tambunan, M. P., 2020. Seagrass distribution using remote sensing along the Ujunggenteng Coastal, Sukabumi. *In IOP Conference Series: Earth and Environmental Science*, 481(1), 012059. https://doi.org/10.1088/1755-1315/481/1/012059

[28] Mahmoud, M. G., El-Khir, E. A., Ebeid, M. H., Mohamed, L. A., Fahmy, M. A., Shaban, K. S., 2020. An assessment on the coastal seawater quality of the Gulf of Suez, Egypt. *Journal of Environmental Protection*, 11(01), 34. https://doi.org/10.4236/jep.2020.111004

[29] Korean Statistical Information Service, 2023. Port water quality status.
https://kosis.kr/statHtml/statHtml.do?orgId=146&tblId=DT_MLTM_1744 (Accessed Dec. 26, 2025)

[30] International Maritime Organization, 2018. Code for Approval of Ballast Water Management Systems (BWMS CODE). Resolution MEPC.300(72), *London, United Kingdom*.

[31] Marine Environmental Protection Committee, 2016. Comments on the Report of the Correspondence Group on the Review of Guidelines (G8) (MEPC 70/4/7).

[32] Moses, G. G., Rao, S. N., Rao, P. N., 2003. Undrained strength behaviour of a cemented marine clay under monotonic and cyclic loading. *Ocean Engineering*, 30, 1765–189. https://doi.org/10.1016/S0029-8018(03)00018-0

[33] Rao, D. K., Raju, G. V. R. P., Sowjanya, C., Rao, J. P., 2009. Laboratory studies on the properties of stabilized marine clay from Kakinada Sea Coast, India. *International Journal of Engineering Science and Technology*, 3(1), 422-428.

[34] Basack, S., Purkayastha, R. D., 2009. Engineering properties of marine clays from the eastern coast of India. *Journal of Engineering and Technology Research*, 1(6), 109-114.

[35] Rahman, Z. A., Yaacob, W. Z. W., Rahim, S. A., Lihan, T., Idris, W. M. R., Sani, W. N. F., 2013. Geotechnical characterisation of marine clay as potential liner material. *Sains Malaysiana*, 42(8), 1081–1089.

[36] Tongwei, Z., Xibing, Y., Yongfeng, D., Dingwen, Z., Songyu, L., 2014. Mechanical behaviour and micro-structure of cement-stabilised marine clay with a metakaolin agent. *Construction and Building Materials*, 73, 51–57. https://doi.org/10.1016/j.conbuildmat.2014.09.041

[37] Otoko, G. R., Simon, A. I., 2015. Stabilization of a deltaic marine clay (chikoko) with chloride compounds: y-values. *International Research Journal of Engineering and Technology*, 2(3), 2092–2097.

[38] Loisel, H., Vantrepotte, V., Jamet, C., Dat, D. N., 2013. Challenges and new advances in ocean color remote sensing of coastal waters. *Topics in oceanography*, 1-38. https://doi.org/10.5772/56414

[39] Fan, H., Wang, X., Zhang, H., Yu, Z., 2018. Spatial and temporal variations of particulate organic carbon in the Yellow-Bohai Sea over 2002–2016. *Scientific Reports*, 8(1), 7971. https://doi.org/10.1038/s41598-018-26373-w

[40] Guo, W., Ye, F., Xu, S., Jia, G., 2015. Seasonal variation in sources and processing of particulate organic carbon in the Pearl River estuary, South China. *Estuarine, Coastal and Shelf Science*, 167, 540-548. https://doi.org/10.1016/j.ecss.2015.11.004

[41] Whitaker, S., 1986. Flow in porous media I: A theoretical derivation of Darcy's law. *Transport in porous media*, 1, 3-25. https://doi.org/10.1007/BF01036523

[42] Coulson, J. M., Richardson, J. F., Backhurst, J. R., Harker, J. H., 1990. Chemical engineering: fluid flow, heat transfer and mass transfer (Vol. 1). *Pergamon Press*.

[43] Siemens, S.C., 2018. STAR-CCM+ Version 13.06-User Guide. Siemens PLM Software.

[44] Cundall, P. A., Strack, O. D. L., 1980. Discussion: A discrete numerical model for granular assemblies. *Géotechnique*, 30(3), 331–336. https://doi.org/10.1680/geot.1980.30.3.331

[45] IMO-MEPC., 2008. Guidelines for approval of ballast water management systems (G8). *London: International Maritime Organization*.

[46] Seo, K. C., Lee, K. W., Rho, B. S., Cho, I. S., Lee, W. J., Pham, V. C., Choi, J. H., 2020. A study on the difference in ballasting time arising from the installation of an ultraviolet ballast water management system on existing ships. *Journal of the Korean Society of Marine Environment & Safety*, 26(5), 576-585. https://doi.org/10.7837/kosomes.2020.26.5.576